

1 Investigating the relationship between volume
2 transport and sea surface height in a numerical
3 ocean model

4 Estee Vermeulen ^{1,2*}, Björn Backeberg ^{2,3,4}, Juliet Hermes ^{1,5}, Shane Elipot ⁶

5 ¹ *Department of Oceanography, University of Cape Town, Rondebosch, South Africa*

6 ² *Nansen-Tutu Centre for Marine Environmental Research, University of Cape Town, South
7 Africa*

8 ³ *CSIR, Coastal Systems Research Group, Stellenbosch, South Africa*

9 ⁴ *Nansen Environmental and Remote Sensing Centre, Bergen, Norway*

10 ⁵ *South African Environmental Observation Network, Egagasini Node, Cape Town, South
11 Africa*

12 ⁶ *Rosenstiel School of Marine and Atmospheric Science, University of Miami, 4600
13 Rickenbacker Causeway, Miami, FL 33149*

14 * *Corresponding author address:* Estee Vermeulen, Department of Oceanography, University of
15 Cape Town, Rondebosch, South Africa

16 Email: esteever01@gmail.com

17 Abstract

18 The Agulhas Current Time-series mooring array (ACT) measured transport of the Agulhas
19 Current at 34°S for a period of 3 years. Using along-track satellite altimetry data directly
20 above the array, a proxy of Agulhas Current transport was developed based on the relationship
21 between cross-current sea surface height (SSH) gradients and the measured transports. In
22 this study, the robustness of the proxy is tested within a numerical modelling framework,
23 using a 34-year long regional-hindcast simulation from the Hybrid Coordinate Ocean Model
24 (HYCOM). The model specifically tested the sensitivity of the transport proxy to (1) changes
25 in the vertical structure of the current and to (2) different sampling periods used to calculate the
26 proxy. Two reference proxies were created using HYCOM data from 2010-2013, by extracting
27 model data at the mooring positions and along the satellite altimeter track for; the box (net)
28 transport and the jet (southwestward) transport. Sensitivity tests were performed where the
29 proxy was recalculated from HYCOM for (1) a period where the modelled vertical stratification
30 was different compared to the reference proxy, and (2) different lengths of time periods: 1, 3,
31 6, 12, 18 and 34 years. Compared to the simulated (native) transports, it was found that
32 the HYCOM proxy was more capable of estimating the box transport of the Agulhas Current
33 compared to the jet transport. This was because the model is unable to resolve the dynamics
34 associated with meander events, for which the jet transport algorithm was developed. The
35 HYCOM configuration in this study contained exaggerated levels of offshore variability in the
36 form of frequently-impinging baroclinic anticyclonic eddies. These eddies consequently broke
37 down the linear relationship between SSH slope and vertically-integrated transport. Lastly,
38 results showed that calculating the proxy over shorter or longer time periods in the model did
39 not significantly impact the skill of the Agulhas transport proxy, suggesting that 3-years was
40 a sufficiently long time-period for the observation based transport proxy. Modelling studies of
41 this kind provide useful information towards advancing our understanding of the sensitivities
42 and limitations of transport proxies that are needed to improve long-term ocean monitoring
43 approaches.

44 1 Introduction

45 The Agulhas Current System is the strongest western boundary current in the Southern
46 Hemisphere and transports warm tropical water southward along the east coast of South
47 Africa [Lutjeharms, 2006]. The Agulhas Current, in the northern region, is known for
48 its narrow, fast, flow conditions following the steep continental slope [de Ruijter et al.,
49 1999]. As the current continues southwestward it becomes increasingly unstable over
50 the widening continental shelf until it eventually retroflects, forming an anticyclonic loop
51 south of Africa and returning to the Indian Ocean as the eastward Agulhas Return Current
52 [Beal et al., 2011; Biastoch and Krauss, 1999; Dijkstra and de Ruijter, 2001; Hermes
53 et al., 2007; Lutjeharms, 2006; Loveday et al., 2014]. The anticyclonic loop, known as
54 the Agulhas Retroflection, contains some of the highest levels of mesoscale variability
55 in the global ocean [Gordon, 2003] in the form of Agulhas rings, eddies and filaments.
56 These contribute to leakage from this region, contributing heat, salt and energy into the
57 Benguela upwelling system, the Atlantic Ocean and the global overturning circulation
58 system [Gordon et al., 1987; Beal et al., 2011; Durgadoo et al., 2013], impacting the
59 Atlantic Meridional Overturning Circulation (AMOC) [Biastoch and Krauss, 1999; Beal
60 et al., 2011; Durgadoo et al., 2013; Loveday et al., 2014]. In the regional context, the
61 Agulhas Current has a major influence on the local weather systems, due to large latent
62 and sensible heat fluxes, which contributes to rainfall and storm events over the adjacent
63 land [Reason, 2001; Rouault et al., 2002; Rouault and Lutjeharms, 2003]. The unique
64 circulation of the Agulhas Current System, in the context of regional and global climate
65 variability, makes it an important field of research.

66 To understand the complicated dynamics of the Agulhas Current requires an integrated
67 approach using numerical ocean models, satellite remote sensing measurements and *in situ*
68 observations. Previous studies have suggested that measuring the dynamics of the Agulhas
69 Current in the northern region is easier due to its stable trajectory and its confinement
70 to the continental slope [van Sebille et al., 2010]. However, the close proximity of the
71 current to the coast has made it difficult to monitor using satellite altimetry [Rouault
72 et al., 2010]. Newer altimetry products dedicated to coastal areas are promising but are
73 yet to be validated within the Agulhas Current region [Birol et al., 2017]. In addition,

74 the frequent disturbances of the current in the form of solitary meanders, also known as
75 Natal Pulses, and its interactions with mesoscale features originating upstream and from
76 the east [Elipot and Beal, 2015], remain poorly resolved in many numerical ocean models
77 [Tsugawa and Hasumi, 2010; Braby et al., 2016], highlighting the challenges involved in
78 monitoring and modelling the dynamics in this region.

79 There is a trade-off between spatial and temporal sampling. *In situ* mooring observa-
80 tions provide high temporal observations of the Agulhas Current throughout the water
81 column but are spatially coarse. In contrast, satellite observations can provide high spa-
82 tial resolution data of the surface ocean but lacks detailed information below the surface.
83 Hence, numerical models are needed to provide a temporally coherent, high resolution
84 representation of the ocean throughout the water column. Numerous studies aiming to
85 monitor long-term changes in global current systems have adopted methods to combine
86 various sampling tools [eg. Maul et al. 1990; Imawaki et al. 2001; Andres et al. 2008; Zhu
87 et al. 2004; Yan and Sun 2015], including the recent development of the Agulhas transport
88 proxy established to monitor the interannual variability and long-term trends in Agulhas
89 Current transport [Beal and Elipot, 2016].

90 Beal and Elipot [2016] have shown that a strong relationship exists between surface geo-
91 strophic velocity and full-depth transport such that sea level anomalies can be used to
92 study the variability and dynamics of the Agulhas Current System as has been demon-
93 strated before [Fu et al., 2010; Rouault et al., 2010; Rouault and Penven, 2011; etc.].
94 The 22-year transport proxy created by Beal and Elipot [2016] assumed a fixed linear
95 relationship between *in situ* transport and sea surface slope based on *in situ* measure-
96 ments over the 3-year sampling period of the Agulhas Current Time-series experiment
97 (ACT) [Beal et al., 2015]. Analyses of the Agulhas Current transport proxy time-series
98 concluded that the Agulhas Current has not intensified over the last two decades in re-
99 sponse to intensified global winds under anthropogenic climate change [Cai, 2006; Yang
100 et al., 2016], but instead has broadened as a result of increased eddy activity [Beal and
101 Elipot, 2016] in agreement with Backeberg et al. [2012]. This could essentially decrease
102 poleward heat transport and increase mixing over the continental shelf, thereby increasing
103 cross-frontal exchange of nutrients and pollutants between the coastal ocean and the deep
104 ocean [Backeberg et al., 2012; Beal and Elipot, 2016].

105 This modelling study recreates the Agulhas transport proxy developed by Beal and Elipot
106 [2016], within a regional HYCOM simulation of the greater Agulhas Current System,
107 aiming to test the sensitivity of using 3 years of *in situ* mooring data to develop a transport
108 proxy as well as the sensitivity of the proxy to changes in the vertical structure of the
109 Agulhas Current. The paper is structured as follows; Section 2 describes the data and
110 methods, it should be noted that this section forms a key part of the paper as the methods
111 of recreating the proxy are an integral component of the study. Section 3 presents the
112 results from the HYCOM transport proxy and lastly Section 4 presents the summary and
113 conclusions.

114 **2 Data and Methods**

115 **2.1 The Hybrid Coordinate Ocean Model**

116 The Hybrid Coordinate Ocean Model (HYCOM) is a primitive equation ocean model
117 that was developed from the Miami Isopycnic Coordinate Ocean Model (MICOM) [Smith
118 et al., 1990]. HYCOM combines the optimal features of isopycnic-coordinate and fixed-
119 grid ocean circulation models into one framework [Bleck, 2002] and uses the hybrid layers
120 to change the vertical coordinates depending on the stratification of the water column.
121 The model makes a dynamically smooth transition between the vertical coordinate types
122 via the continuity equation using the hybrid coordinate generator [Chassignet et al., 2007].
123 Well-mixed surface layers use z-level coordinates, ρ -coordinates are utilized between the
124 surface and bottom layers in a well-stratified ocean, and the bottom layers apply σ -
125 coordinates following bottom topography. Adjusting the vertical spacing between the
126 hybrid coordinate layers in HYCOM simplifies the numerical implementation of several
127 physical processes without affecting the efficient vertical resolution, and thus combines
128 the advantages of the different coordinate types in optimally simulating coastal and open-
129 ocean circulation features [Chassignet et al., 2007].

130 This study used output from a one-way nested $1/10^\circ$ model of the greater Agulhas Current
131 System (AGULHAS) [Backeberg et al., 2008; 2009; 2014]. The regional nested model,
132 AGULHAS, received boundary conditions from the basin-scale model of the Indian and
133 Southern Ocean (INDIA) [George et al., 2010] every 6-hrs. The boundary conditions

134 were relaxed towards the outer model over a 20 grid cell sponge layer. The nested model
135 covered the region from the Mozambique Channel to the Agulhas Retroflexion region
136 and the Agulhas Return Current, geographically extending from approximately 0°-60°
137 East and from 10°-50° South, with a horizontal resolution of ~ 10 km that adequately
138 resolved mesoscale dynamics to the order of the first baroclinic Rossby radius estimated
139 to be about 30 km [Chelton et al., 1998]. AGULHAS has 30 hybrid layers and targeted
140 densities ranging from 23.6 to 27.6 kg/m³.

141 AGULHAS was initialised from a balanced field of the parent model interpolated to the
142 high-resolution grid and ran from 1980 to 2014 using interannual forcing from ERA40
143 [Uppala et al., 2005] and ERA-interim [Dee et al., 2011]. Version 2.2 of the HYCOM source
144 code has been used in this model and, together with the second order advection scheme,
145 provides an adequate representation of the Agulhas Current [Backeberg et al., 2014].
146 However, limitations of the free running model include high levels of SSH variability south
147 of Madagascar and offshore of the Agulhas Current, suggesting that eddy trajectories may
148 be too regular in the model [Backeberg et al., 2014]. The data available for this study
149 was a weekly output of the regional HYCOM model of the Agulhas region from 1980 to
150 2014.

151 **2.2 The Agulhas Current Time-series Experiment**

152 The ACT experiment was established to obtain a multi-decadal proxy of Agulhas Current
153 transport using satellite altimeter data. The first phase of the experiment was the *in situ*
154 phase where the ACT mooring array was deployed in the Agulhas Current, near 34°S,
155 for a period of three years from: 2010-2013 [Beal et al., 2015] (Figure 1). From the
156 data collected, Beal et al. [2015], provided two volume transport estimates: (1) a box or
157 boundary layer transport (T_{box}) and (2) a western boundary jet transport (T_{jet}). T_{box} is
158 the net transport within a fixed distance from the coast, while T_{jet} is a stream dependent
159 transport that is calculated by changing the boundaries of integration at each time step
160 depending on the strength and cross-sectional area of the southwestward jet. The western
161 boundary jet transport algorithm was developed to specifically exclude the northeastward
162 transport during meander events, occurring inshore of the meander [Beal et al., 2015].

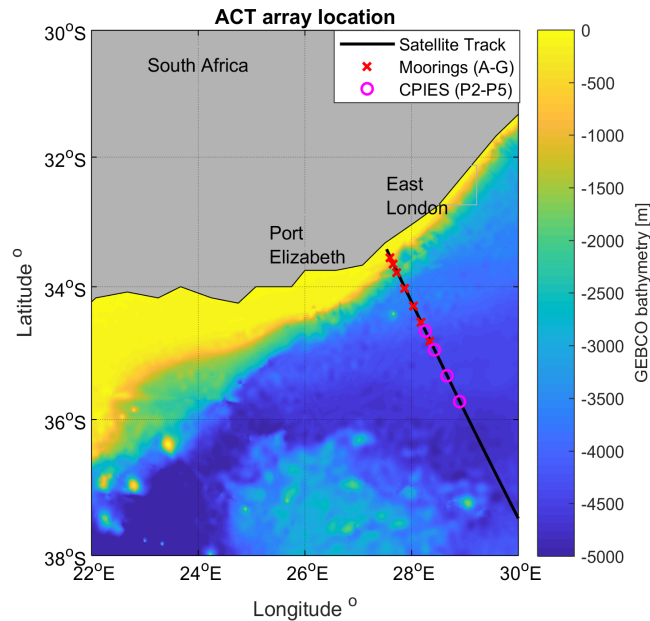


Figure 1: Geographical location of the ACT array with the mooring (red crosses) and CPIES (magenta circles) stations relative to the T/P, Jason-1,2,3 satellite track #96 (black line). Colour shading illustrates the GEBCO bathymetry (m).

163 During the second phase of the ACT experiment, Beal and Elipot [2016] built a 22-year
 164 transport proxy by regressing the three years of *in situ* transport measurements (obtained
 165 from phase 1) against along-track satellite altimeter data spanning the years 1993-2015.

166 2.3 Development of the Agulhas transport proxy

167 Previous analyses have shown that the vertical structure of the Agulhas Current is baro-
 168 tropic [Elipot and Beal, 2015], implying that the relationship between surface geostrophic
 169 velocity and full depth transport should be strong, despite the presence of the Agulhas
 170 Undercurrent [Beal and Elipot, 2016] (Figure 2). Access to the data from the ACT ex-
 171 periment allowed us validate the velocity cross-section in HYCOM (Figure 2). Beal et al.
 172 [2015] defined the Agulhas Current to be 219 km wide and 3000 m deep on average, as is
 173 reflected in the vertical section of the *in situ* ACT observations (Figure 2a). In HYCOM
 174 the current appears to be wider, weaker and further offshore than the observed current,
 175 on average the current is 254 km wide and extends deeper down to ~ 3500 m, particularly
 176 inshore, with a less pronounced undercurrent (Figure 2b).

177 The transport proxy created by Beal and Elipot [2016] was initially developed by finding
 178 a linear relationship between transport and sea surface slope across the entire length

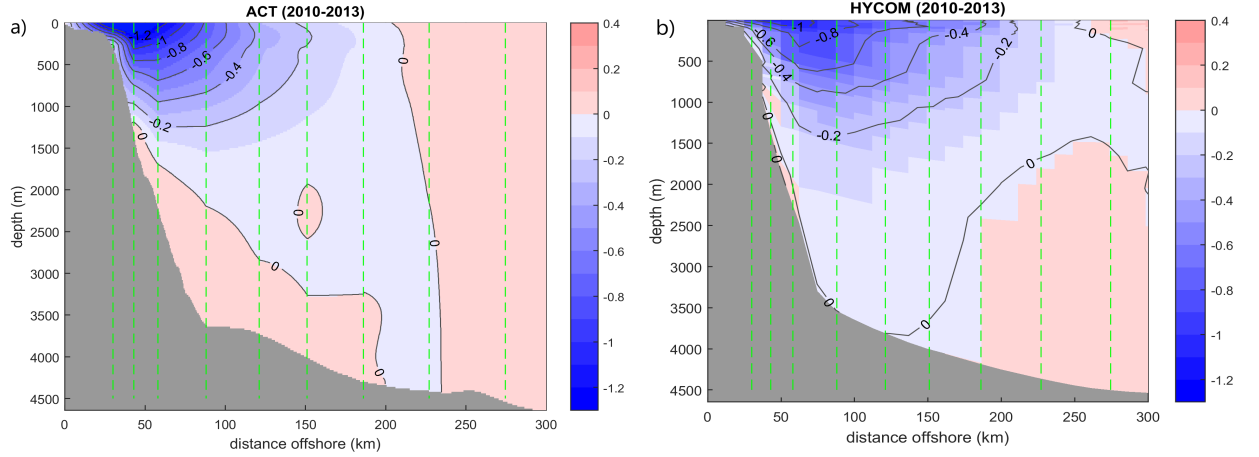


Figure 2: Time mean cross-section of the velocity structure of the Agulhas Current across the ACT array (ms^{-1}) during the *in situ* ACT period (2010-2013) from (a) the ACT Observations (b) the HYCOM-AGULHAS simulation. Blue shading represents the negative, southwest current direction and pink shading represents the positive, northeast current flow. Contours are every $0.2 ms^{-1}$. Dashed green vertical lines represents the nine locations of the mooring and CRIES-pairs, the first line representing mooring A and CRIES-pair P4P5 furthest offshore.

179 of the ACT array, a common method used in previous studies [Imawaki et al., 2001;
 180 van Sebille et al., 2010; Sprintall and Revelard, 2014; Yan and Sun, 2015]. However,
 181 this method lead to uncertainty in the linear regression due to the strong, co-varying
 182 sea surface height across the current. The preferred method was therefore to build nine
 183 individual linear regression models, one for each mooring position and CRIES-pairs along
 184 the ACT array, which locally related transport to sea surface slope [Beal and Elipot,
 185 2016]. It is important to note that the regression models assumed a constant, linear
 186 relationship between sea surface slope and transport over the three-year *in situ* period.
 187 The transport variable in the regression models was defined as transport per unit distance,
 188 i.e. the vertically integrated velocity with units in m^2s^{-1} , where T_x represents the net
 189 component of the current flow and T_{xsw} the southwestward component of the flow. The
 190 total transports, T_{box} and T_{jet} in m^3s^{-1} , were calculated by integrating the T_x and T_{xsw}
 191 estimates, predicted from the regression models, to the respective current boundaries.

192 2.4 Recreating the Agulhas transport proxy in HYCOM

193 In order to recreate the Agulhas Current proxy in HYCOM, data corresponding to the
 194 measurements collected from the ACT mooring array were extracted from the model. To
 195 build the regression models the transport per unit distance and sea surface slope for each
 196 of the nine mooring locations were calculated using the model data (hereafter CRIES

197 pairs P3-P4 and P4-P5 were included as mooring positions 8 and 9).

198 **2.4.1 Model Transport**

199 The barotropic velocity -equivalent to an integral of the velocity with depth- from each
200 mooring location (A-G) and CPIES pairs P3-P4 and P4-P5 [Beal et al., 2015] was ex-
201 tracted for the 34-year model period. Extracting the barotropic velocity component from
202 each mooring avoided interpolation errors that may have occurred if the model velocity
203 was interpolated onto the locations of each current-meter instrument on each mooring
204 [e.g. van Sebille et al., 2010]. Transport per unit distance (Tx) for each mooring was cal-
205 culated by multiplying the cross-track barotropic velocity by the respective depth at each
206 mooring location. The same method was employed to calculate the southwest transport
207 component ($Txsw$) excluding the northeast cross-track barotropic velocity values in the
208 calculation.

209 **2.4.2 Model SSH**

210 In order to reproduce the “along-track” SSH altimeter data needed to create the proxy as
211 in Beal and Elipot [2016], 34 years of HYCOM SSH was linearly interpolated onto the
212 coordinates of the TOPEX/Jason satellite track number 96 overlapping the model ACT
213 array. The coordinates of the along-track altimeter data were obtained from the filtered
214 12 km Jason-2 Aviso satellite product. To obtain the sea surface slope for each regression
215 model, an optimal pair of SSH data points was chosen such that the horizontal length
216 scale between them allowed for a maximum correlation between sea surface slope and Tx .
217 The length scales of the slopes ranged from 24 km at mooring A to 12 km at mooring
218 G and 48 km for the offshore CPIES-pairs, indicating an increase in the spatial scale
219 of offshore flow, possibly due to increased offshore variability. Results from the *in situ*
220 proxy experiment by Beal and Elipot [2016] also showed an increasing length scale with
221 increasing distance offshore, however the results varied in magnitude: 27 km at mooring B
222 to 102 km at mooring G. In this study the SSH slope was calculated such that a negative
223 SSH slope corresponds to a negative surface velocity (southwest) according to geostrophy,
224 whereas a positive slope would indicate positive northeastward flow.

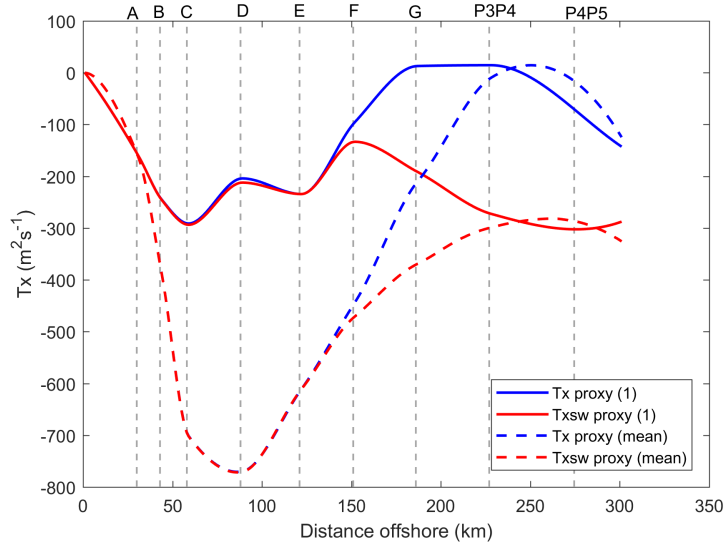


Figure 3: HYCOM transport per unit distance proxy ($\text{m}^2 \text{s}^{-1}$) for T_x (blue) and T_{xsw} (red) at 1 km intervals at the first model time step (solid lines) and for the ACT reference period (2010-2013, dashed lines). The grey dashed-lines represent the positions of moorings and offshore CPIES pairs.

2.4.3 Building the regression models

Nine linear regression models were developed to estimate the transport per unit distance (T_x and T_{xsw}) from the HYCOM sea surface slope during the same three-year period over which the ACT proxy was developed (April 2010- February 2013). The three-year time period is hitherto referred to as the reference period.

To calculate the total transport across the ACT array required continuous T_x estimates across the current. This was achieved as in Beal and Elipot [2016] by fitting a piecewise cubic Hermite interpolating polynomial function to obtain transport estimates at 1 km intervals from the coast to the end of the array (Figure 3). Fitting the transport function to the coast and equating it to zero would be equivalent to implementing a no slip boundary condition in the model. Before calculating the total transport the current boundaries needed to be defined. The box transport (T_{box}) was calculated by integrating T_x horizontally to 230 km offshore, the three-year mean width of the current in HYCOM. The jet transport (T_{jet}) was calculated using the algorithm developed by Beal et al. [2015] by integrating T_{xsw} , the southwest transport component, to the first maximum of T_x beyond the half-width of the current (115 km in HYCOM) at each time step (Figure 3).

241 Assuming that the three-year linear relationship between SSH slope and transport per
 242 unit distance (T_x and T_{xsw}) from 2010-2013 remains constant, the regression models
 243 were applied to the entire 34-year SSH model data. Thereafter, the 34-year transports
 244 were calculated by applying the same methods that were used to calculate the 3-year
 245 transport time-series; firstly, obtaining T_x and T_{xsw} estimates at 1 km-intervals along
 246 the array and secondly integrating horizontally to obtain T_{box} and T_{jet} .

247 **2.5 Comparison of the transport proxy to actual model transports**

248 The simulated model transports were calculated using the full-depth velocity fields across
 249 the array. If the relationship between SSH slope and transport is strong, there would be
 250 good agreement between the proxy and the actual model transports. To quantify this,
 251 correlations and transport statistics for the model and proxy were calculated from the two
 252 time-series (Table 2). These provided insight into which processes the proxy may have
 253 failed to capture, which were then further investigated in HYCOM. Statistics are deemed
 254 significant at the 95% significance level.

255 Eddy kinetic energy (EKE) was calculated to show the surface variability of the current
 256 coincident with averaged SSH contours used to represent the mean surface structure
 257 (Figure 6). EKE was calculated over the 3-year mean reference period, and over the
 258 highest and lowest correlated years. In order to evaluate the subsurface current structure
 259 along the ACT array, vertical velocity profiles were analysed for each mooring and CRIES-
 260 pair over the 3-year mean reference period as well as over the highest and lowest correlated
 261 years.

262 Transport variability in HYCOM was analysed by investigating the current structure
 263 during the residual transport events in the least and best performing regression models.
 264 Residual transport events were identified as the outlying residual transport values above
 265 and below 2 standard deviations of the estimated transport.

$$e = Txi - \hat{Txi} \quad (1)$$

266 where e is the estimated residuals, Txi is the HYCOM transport per unit distance value
 267 and \hat{Txi} is the estimated transport per unit distance value according to the linear regres-

268 sion models (i.e the transport proxy).

269 To investigate the current structure during these residual events, composite averages of
270 the cross-track velocity structure were analysed. The cross-track velocity at each depth
271 layer in HYCOM was extracted at 12 km intervals from 0 km to 400 km offshore, for the
272 34-year model period. Although the ACT array only reached 300 km offshore, analysis of
273 the current structure in HYCOM was extended further offshore. Previous analyses have
274 shown increased levels of offshore variability in this HYCOM simulation [Backeberg et al.,
275 2009; 2014], which therefore made it interesting to study the subsurface structure during
276 the offshore current meanders and the influence these could have on the transport proxy.
277 To further investigate the effect of the residual transport values on the transport proxy,
278 all corresponding transport events exceeding plus or minus two standard deviations were
279 removed from each linear regression model during development of the proxy (Figure 4).

280 **2.6 Sensitivity tests**

281 Sensitivity experiments were performed in HYCOM to test how many years of mooring
282 data is needed to create an accurate proxy of Agulhas Current transport. With 34 years
283 of model data the linear relationship could be tested over much longer or shorter periods.
284 Using the method described in section 2.4.3, the proxy regression models were built using
285 1, 6, 12, 18 and 34 years of HYCOM data. In addition, the proxies were calculated over
286 two arbitrary 3-year periods, to test the sensitivity of the proxy to current dynamics
287 over different years. Lastly, the regression models were calculated over the maximum and
288 minimum annual transport years in HYCOM, as well as during the years the HYCOM
289 transport standard deviation was the largest and the smallest. Table 1 shows the time
290 range over which the sensitivity experiments were performed.

Table 1: Sensitivity experiment time periods.

Time range (years)	Model dates
1	Jan 2011 - Dec 2011
3	Apr 2010 - Feb 2013
6	Jan 2009 - Dec 2014
12	Jan 2003 - Dec 2014
18	Jan 1997 - Dec 2014
34	Jan 1980 - Dec 2014
3*	Jan 1980 - Dec 1982; Jan 2000 - Dec 2002
Max (Min) HYCOM transport.	2003 (1982)
Max (Min) HYCOM transport STD.	2013 (1980)

3* Corresponds to the two additional 3-year periods

291 3 Results

292 3.1 HYCOM linear regression models

293 The coefficient of determination (R^2) from the regression models highlight how well the
294 linear relationship predicts the transport in HYCOM (Figure 4). R^2 ranged from 0.86 at
295 mooring A (30 km offshore) to 0.49 at the last CPIES-pair P4P5 (275 km offshore) for
296 T_x and 0.86 at mooring A to 0.37 at P4P5 for T_{xsw} (P values $< 10^{-3}$). Results from Beal
297 and Elipot [2016] showed an increase in the R^2 statistics in the regression models ranging
298 from 0.51 at mooring A and 0.81 for CPIES-pair P4P5 for T_x , indicating that the *in situ*
299 observation based regression models had poorer skill inshore, whereas in HYCOM the
300 regression models have poorer skill offshore. The results from the T_{xsw} regression models
301 in HYCOM showed similar results to Beal and Elipot [2016] for the inshore mooring
302 locations (A, B, C, E) with slightly higher correlations for offshore moorings F, G and
303 CPIES-pair P3P4 but a lower correlation for D and the furthest CPIES-pair P4P5.

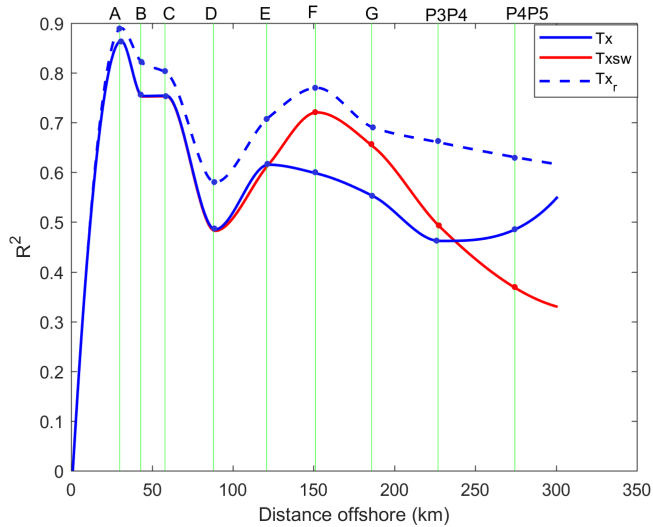


Figure 4: R^2 statistics from the linear regression models showing the relationship between HYCOM SSH slope and HYCOM transport per unit distance for each mooring (A-G) and CRIES-pair (P3P4 & P4P5) over the 3-year reference period (2010-2013). T_x is represented by the solid blue line and T_{xsw} by the solid red line. The dashed blue line represents the results of T_x after the removal of the residual transport events (see section 3.4). Sites A - CRIES pair P4P5 are shown by the faint green lines.

304 3.2 Proxy validation

305 Two transport types, the box transport (T_{box}) and the jet transport (T_{jet}) were extracted
 306 from HYCOM in order to validate the relative proxies. The T_{box} (T_{jet}) proxy explained
 307 57% (14%) of transport variance during the three-year reference period (2010-2013) (Table
 308 2b). Using 34-years of model data (1980-2014), assuming the fixed 3-year relationship
 309 between SSH slope and transport, T_{box} (T_{jet}) explained 52% (26%) of the transport
 310 variance (Table 2b). Results from Beal and Elipot [2016] also showed that T_{box} explained
 311 a higher percentage of variance (61%) during the ACT period than the jet transport proxy
 312 (T_{jet} : 55%).

313 The 34-year mean transport and standard deviation from HYCOM for T_{box} and T_{jet} was
 314 -84 ± 47 Sv and -110 ± 38 Sv respectively (Table 2a). The proxy T_{box} and T_{jet} was -87
 315 ± 34 Sv and -92 ± 31 Sv respectively (Table 2a). According to the ACT observations
 316 the mean transport and standard deviation was -77 ± 32 Sv for T_{box} and -84 ± 24 Sv for
 317 T_{jet} . A higher jet transport was expected considering it excludes northeast counter-flows
 318 that decrease the box transport [Beal et al., 2015]. The differences between the standard
 319 deviations of HYCOM and the proxy indicate that transport in HYCOM experiences more

Table 2: a) Summary of the transport statistics of the ACT observations over the 3-year *in situ* period and the HYCOM model transports and HYCOM proxy transports over the 3-year and extended 34-year time period. Negative values denote transport in the southwest direction. 1 Sv=10⁶ m³s⁻¹. b) Correlations between the HYCOM model transport and HYCOM proxy transport, for the box transport and jet transport with the percentage of variance shown in brackets. All correlations were significant.

a)	ACT (2010-2013)		HYCOM (2010-2013)		Proxy		HYCOM (1980-2014)		Proxy	
Transport	T_{box}	T_{jet}	T_{box}	T_{jet}	T_{box}	T_{jet}	T_{box}	T_{jet}	T_{box}	T_{jet}
Mean & Std (Sv)	-77 ± 32	-84 ± 24	-81 ± 53	-112 ± 41	-91 ± 35	-92 ± 30	-84 ± 47	-110 ± 38	-87 ± 34	-92 ± 32
Max (Sv)	-157	-174	-223	-244	-196	-185	-236	-245	-213	-219
Min (Sv)	23	-25	44	-48	-36	-46	87	-30	-20	-27

b)	T_{box}	T_{jet}
2010-2013	0.75 (57%)	0.38 (14%)
1980-2014	0.72 (52%)	0.51 (26%)

320 variability compared to the proxy. The proxies only capture a portion of the transport
321 estimate from HYCOM, suggesting it also only captures a portion of the model variability.
322 The positive minimum transport values for T_{box} during both time periods also appear to
323 be peculiar, suggesting a current reversal during those events (Table 2a).

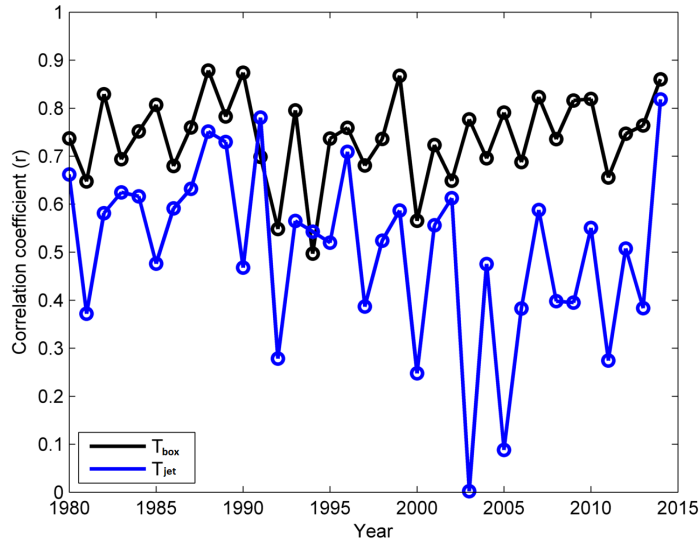


Figure 5: 34-year annual correlations between the box (black) and jet (blue) transport proxies against the box and jet transports extracted from HYCOM.

324 The T_{jet} annual correlation varies greatly from year to year with a significant maximum
325 correlation of 0.82 (2014) and a minimum correlation of 0.00 (2003) (Figure 5). In con-

326 trast, the correlations for T_{box} vary much less and are always significant with a maximum
327 correlation of 0.88 (1988) and minimum correlation of 0.50 (1994) (Figure 5). The box
328 transport has higher correlations for most of the 34-year time period except during two
329 single years where the jet transport has a higher correlation, 0.78 versus 0.70 during 1991
330 and 0.54 versus 0.50 during 1994. These results indicate that the proxy is generally better
331 suited in HYCOM to estimate the box transport rather than the jet transport.

332 The jet transport proxy by Beal and Elipot [2016] was developed to estimate the transport
333 of the Agulhas Current during mesoscale meander events, which generally causes the
334 current to manifest as a full-depth, surface intensified, cyclonic circulation out to 150 km
335 from the coast with anticyclonic circulation farther offshore [Elipot and Beal, 2015]. The
336 Agulhas meanders in the HYCOM simulation occur in association with large anticyclonic
337 eddies predominantly located at the offshore edge of the current, with a narrow, southwest
338 stream close to the coast [Backeberg et al., 2009]. In some instances anticyclonic eddies
339 span the length of the entire array. Therefore, considering that the model is unable to
340 resolve the dynamics associated with meander events, for which the jet transport algorithm
341 was specifically developed, further analysis only focuses on the box transport proxy.

342 **3.3 Evaluating the net transport proxy**

343 The strengths and weaknesses of the box proxy are further investigated by selecting the
344 highest and lowest correlated years from the 34-year annual correlations (Figure 5), and
345 evaluated by plotting the current structure in the model over the respective years (Figures
346 6 & 7).

347 During the year with maximum correlation (1988) the current is stable and inshore,
348 whereas during the lowest correlated year (1994) and during the proxy reference period
349 (2010-2013) the current is meandering and it appears that a large portion of the energy
350 of the current has been shifted offshore (Figure 6). The narrow spacing of the SSH
351 contours for all three periods indicates a strong gradient inshore and hence a strong
352 mean geostrophic current, however the wide spacing between the SSH contours offshore
353 suggests that the variability in the model is confined to the offshore side of the current.
354 It is assumed that high levels of mesoscale variability in the model could bias the current
355 position and hence the transport estimate. However, based on the analysis there were ~ 5

356 anticyclonic eddies during the highest correlated year (1988) and ~ 7 anticyclonic eddies
357 during the lowest correlated year (1994) which does not explain the difference in the
358 accuracy of the proxy for those years.

359 The model cross-track velocity changes direction with depth, specifically for offshore moor-
360 ing G and CPIES-pairs P3P4 and P4P5, at the depth of ~ 2000 m (Figure 7) thereby
361 defining the depth of the Agulhas jet. During the 3-year reference period the velocity
362 changes direction at moorings B and G (~ 1200 m and ~ 2000 m respectively) and at
363 sites P3P4 (~ 2000 m) and P4P5 (~ 300 m, ~ 2000 m). During 1988, sites F-P4P5 exper-
364 ience a change in direction ($> \sim 2000$ m). Lastly, during 1994 mooring G and sites P3P4
365 and P4P5 exhibit a change in direction ($> \sim 2000$ m). An explanation for the offshore
366 subsurface countercurrents may be due to the impinging baroclinic eddies continuously
367 propagating downstream [Backeberg et al., 2009], affecting the entire water column by
368 changing the direction of flow at certain depths. This directly impacts the accuracy of the
369 proxy and explains why the transport proxy fails to capture current reversals (Table 2),
370 because the SSH slope does not capture the subsurface countercurrents associated with
371 the impinging baroclinic eddies.

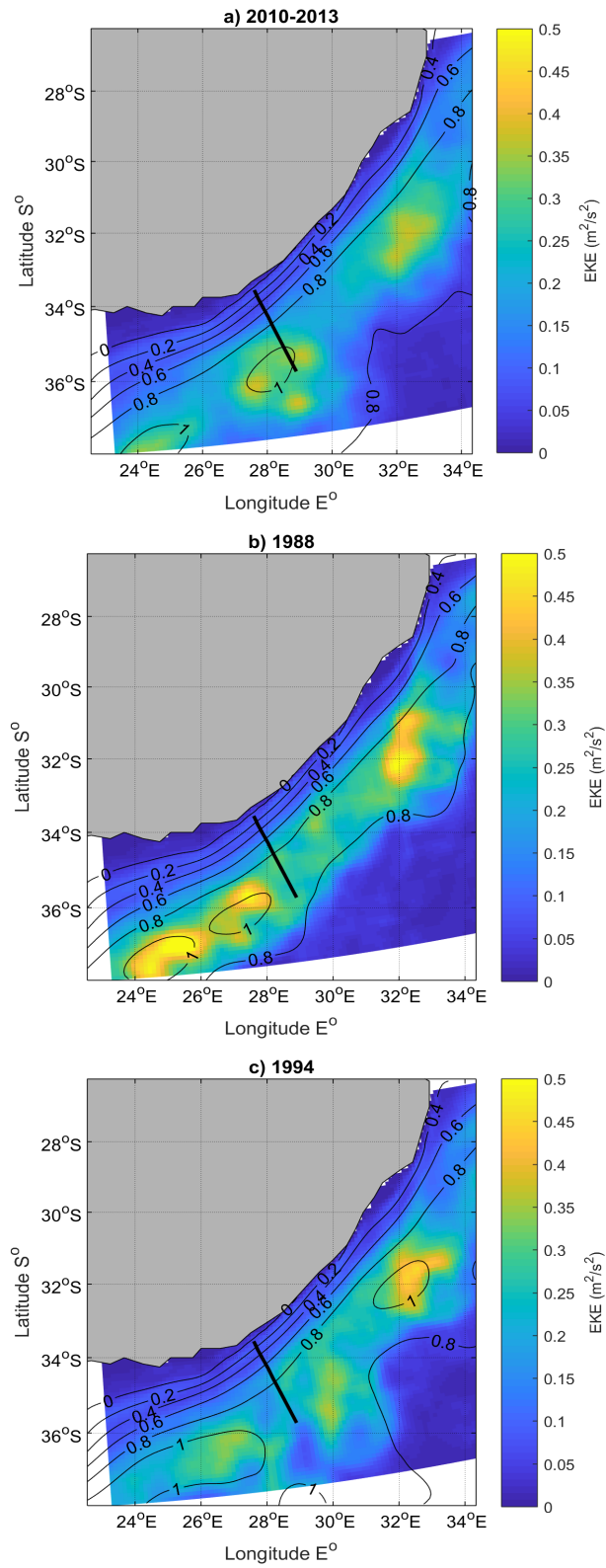


Figure 6: Eddy kinetic energy (EKE in m^2s^{-2}) and sea surface height (SSH in m) contours during (a) the reference period (2010-2013) (b) the highest (1988) and (c) lowest (1994) correlated years. The black line representing the ACT array.

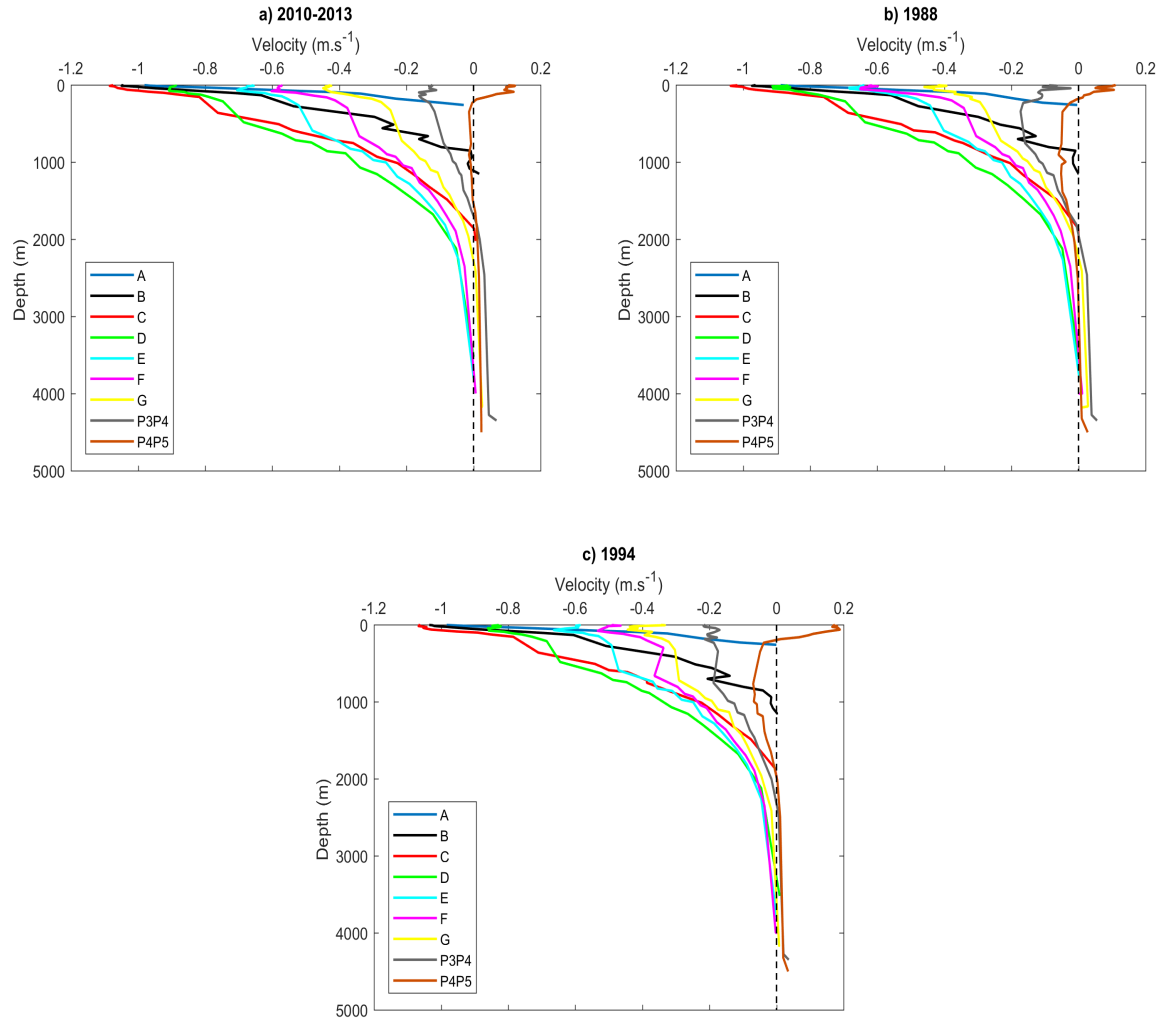


Figure 7: Mean cross-track velocity profiles (m s^{-1}) during (a) the 3-year reference period (2010-2013), (b) during the highest correlated year (1988) and (c) the lowest correlated year (1994). Each colour represents the different moorings (A-G) and CPIES-pairs (P3P4 & P4P5) . Negative values indicate southwestward flow.

372 3.4 Investigating the transport variability

373 As shown previously, the performance of the linear regression models weakened moving
 374 offshore (Figure 4). Regression model, RM8 (CPIES-pair P3P4, Figure 8a) captured the
 375 least transport variance at 46% and RM 1 (mooring A, Figure 8b) explained the most
 376 transport variance at 86%. According to our methods, a negative SSH slope in HYCOM
 377 corresponds to a negative (southwest) surface velocity and if the current structure were
 378 barotropic, a negative (southwest) transport and vice versa.

379 As shown in RM 1 (Figure 8b), all the data points are clustered such that the negative SSH
 380 slope relates to a negative T_x value, in the absence of northeast counterflows. Careful

381 analyses of RM 8 indicates that eight of the nine residual transport events violate the
 382 proportional relationship between SSH slope and Tx (Figure 8a). Some of which have a
 383 negative SSH slope relating to a positive Tx value where others show a positive SSH slope
 384 with negative Tx value. Therefore the SSH slope does not always reflect the direction of
 385 flow at depth, and thus the correct sign for Tx .

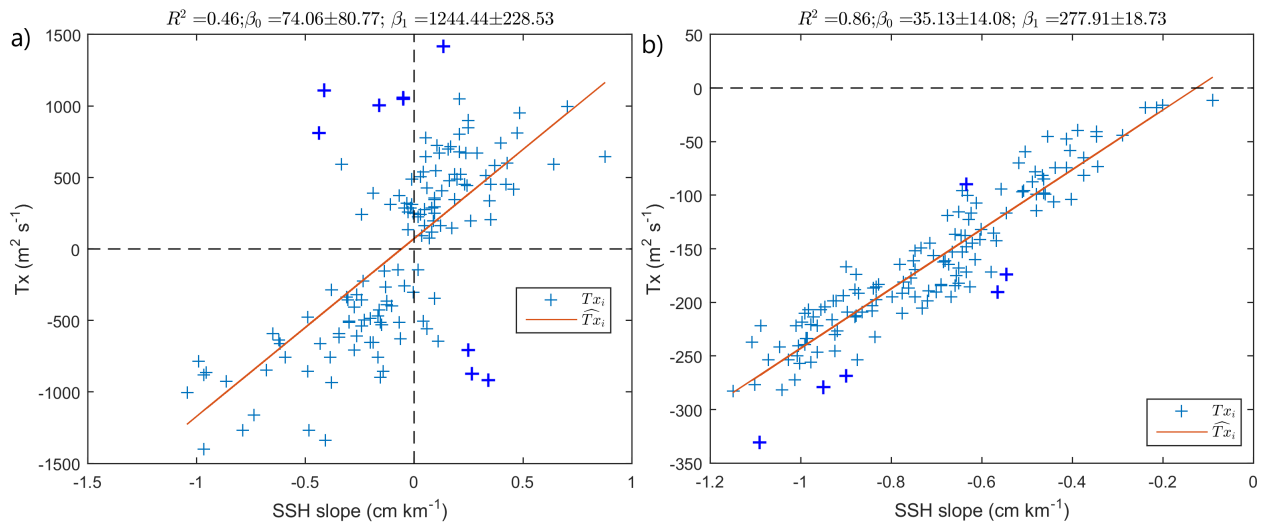


Figure 8: Linear regression models showing the relationship between HYCOM SSH and transport per unit distance (Tx) for a) RM 8; capturing the least transport variance (46%) and b) RM 1; capturing the most transport variance (86%). Txi (blue crosses) represent the Tx values from HYCOM and \hat{Txi} (red line) represents the Tx estimates from the linear regression model. The bold crosses highlight the residual transport events with transport values greater or less than 2 standard deviations of the transport estimate. The coefficient of determination (R^2) quantifies the amount of variance explained by the regression model, β_i is the slope coefficient and β_o the intercept with 95% confidence intervals. Note the different scaling on the x & y-axes.

386 It was expected that removing the outlying transport events (outliers larger than ± 2
 387 standard deviations) would increase the statistical performance of the linear regression
 388 models (Figure 4). However, it is noteworthy that the improvement was remarkably better
 389 for the offshore regression models, since the baroclinic eddies responsible for breaking down
 390 the linear relationship between SSH slope and transport frequently effected the offshore
 391 edge of the current.

392 Examination of the composite cross-track velocity structure of the residual transport
 393 events (Figure 9) shows that there is a change in the direction of velocity in the bottom
 394 layers at the location of RM 8 (CPIES-pair P3P4). The cross-track flow in the surface
 395 layers ($\sim 0-700$ m) of the current is southwestward, whereas below ~ 700 m the flow is
 396 northeastward. Therefore, the vertically integrated flow (Tx) is positive (northeastward)

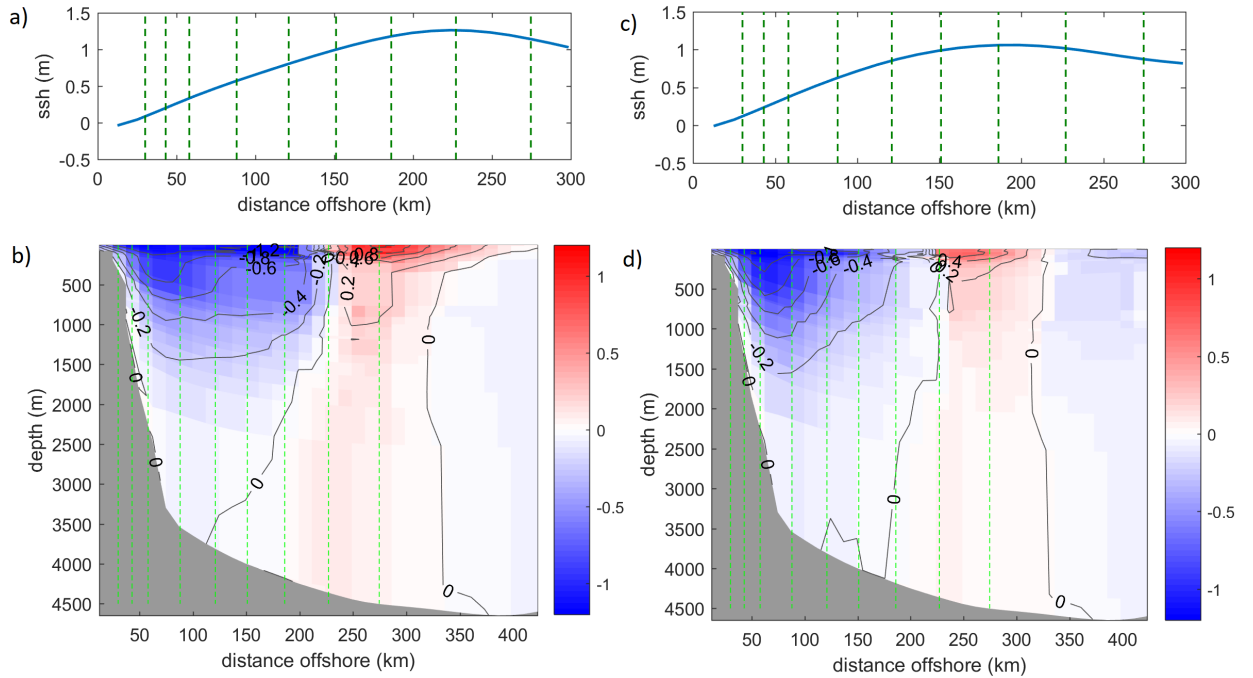


Figure 9: Mean SSH (m) and composite cross-track velocity structure (ms^{-1}) of the residual transport events from RM 8 (a & b) and RM 1 (c & d). Blue shading represents the negative, southwest current direction and red represents the positive, northeast current flow. Contours are every $0.2 ms^{-1}$. Dashed vertical lines represents the nine locations of the mooring and CPIES-pairs, the first line representing mooring A and CPIES-pair P4P5 furthest offshore.

397 and in the opposite direction implied by the SSH slope. In contrast, at mooring A (RM
 398 1), the composite velocity field is always southwestward, consistent with the SSH slope.

399 3.5 Sensitivity tests

400 The 34-year Agulhas transport proxy under analysis thus far was based on regression
 401 models built using only 3 years of HYCOM model data. The statistics in Table 3 show
 402 the results obtained from building the linear regression models and deriving the transport
 403 proxy using 1, 3, 6, 12, 18 and 34 years of model data. We find that the correlation
 404 between proxy box transport and model box transport is not improved by using more
 405 years of model data to build the proxy. Using data from 2010-2013 the correlation of 0.72
 406 changes by no more than 0.01 when extending the number of years of model data (Table
 407 3). Similarly, building the proxy with one year of model data decreases the correlation by
 408 only 0.01 (Table 3). The only difference was the decrease in standard deviation.

Table 3: Transport statistics and correlation results obtained from calculating the box transport proxy over a range of time periods.

Net transport	Transport (Sv)	STD (Sv)	RMSE (Sv)	r
MODEL	-84.32	47.23	0	1.00
1-yr	-87.26	35.47	33.36	0.71
3-yr	-87.21	34.09	32.76	0.72
6-yr	-87.04	35.91	33.04	0.72
12-yr	-86.91	32.51	32.83	0.72
18-yr	-88.71	31.28	32.95	0.72
34-yr	-88.15	29.74	33.14	0.72
1980-1982	-87.86	26.80	34.14	0.70
2000-2002	-94.80	30.31	32.87	0.72

409 The sensitivity of the box transport proxy was also tested using two arbitrary 3-year peri-
410 ods. In comparison to the correlation obtained during 2010-2013 the correlation decreased
411 by 0.02 during 1980-1982 and remained the same during 2000-2002. The results obtained
412 from calculating the T_{box} proxy during the maximum (minimum) transport and standard
413 deviation years in HYCOM showed no improvement or decrease in the skill of the proxy
414 either.

415 4 Summary and conclusions

416 The Agulhas Current transport proxies, developed by Beal and Elipot [2016], were based
417 on nine linear regression models, each assuming a constant linear relationship from three
418 years of observations between *in situ* transport and satellite along-track sea surface gradi-
419 ents. Applying constant linear models and assuming a constant vertical current structure,
420 the transport proxies were extended using 22-years of along-track satellite data to pro-
421 duce two 22-year time-series of Agulhas Current transports [Beal and Elipot, 2016]. The
422 Agulhas Current transport proxies in this study replicates the methods used by Beal and
423 Elipot [2016] but applies these using a regional HYCOM model of the Agulhas Current
424 [Backeberg et al., 2009; 2014].

425 The HYCOM transport proxies were developed using nine, three-year linear regression
426 models between model transport and model SSH slope, and extended using 34-years
427 of the model SSH data from 1980 to 2014. The HYCOM model provided the means to
428 investigate the validity of the assumptions used to create the proxies, such as the constant
429 vertical structure of the current, hence a constant relationship between SSH slope and

430 transport per unit distance during the 3-year reference period and secondly, the temporal
431 scale of observations needed to build a strong linear relationship between transport and
432 SSH slope.

433 Overall, results showed that the proxy was more capable of estimating the box transport
434 (net transport) over the 34 model period, explaining 52% of the transport variance in
435 comparison to 26% of the jet transport (southwest transport) variance. A limitation of
436 this study is that HYCOM was unable to resolve all of the observed dynamics in the
437 Agulhas Current, specifically the mesoscale meander events. The model demonstrated
438 much higher levels of mesoscale variability than observed [Backeberg et al., 2008; 2009].
439 On average, 1.6 mesoscale meanders pass through the ACT array at 34°S per year [Rouault
440 and Penven, 2011; Elipot and Beal, 2015]. In HYCOM, an average of 5 anticyclonic eddies
441 passed over the array per year. The poorer performance of the T_{jet} proxy in HYCOM
442 (26%) compared to the *in situ* T_{jet} proxy (55%) of Beal and Elipot [2016] is due to various
443 model discrepancies including the consistent merging of the anticyclonic eddies with the
444 Agulhas Current in the northern region [Backeberg et al., 2014], which is due to poorly
445 resolved eddy interactions and dissipation processes [Braby et al., 2016], a limitation of
446 many numerical ocean models in this region [Tsugawa and Hasumi, 2010; Penven et al.,
447 2011; Durgadoo et al., 2013; Backeberg et al., 2014; Loveday et al., 2014].

448 Furthermore, although the resolution of HYCOM is able to capture the mesoscale dy-
449 namics of eddies [Holton et al., 2017], it fails to resolve the near-coastal features, such as
450 the inshore, surface intensified cyclonic motion in this simulation. This would require a
451 finer resolution at the coast, in order to reveal smaller offshore displacements, ~50 km,
452 associated with these meander events [Elipot and Beal, 2015]. The poorer performance of
453 the T_{jet} proxy in HYCOM and possibly in the *in situ* study, may also be because it only
454 represents the southwestward component of the flow, whereas the input sea surface slope
455 reflects the net flow along the array. Therefore, based on these findings further analysis
456 focused on the T_{box} proxy only.

457 The frequently impinging eddies have been found to make it difficult to effectively estim-
458 ate the accurate box transport of the Agulhas Current in the model since the advection of
459 these eddies are responsible for large transport fluctuations [Backeberg et al., 2009]. The
460 transport proxy only included the transport of the portion of the eddy that was reflected

461 in the SSH signal across the array, whether it was the southwestward or northeastward
462 portion of the eddy or both. Although the transport proxy may capture the SSH signal
463 of the eddies along the array, the correlation of the regression models decreases offshore.
464 Therefore transport estimates inshore would be more accurate than the transport estim-
465 ates offshore when the current is in a meandering state.

466 It was shown that removing the residual transport events, violating the proportional re-
467 lationship between SSH slope and transport as a result of impinging baroclinic eddies,
468 improved the proxy performance i.e. increased the percentage of transport variance ex-
469 plained. Several studies have suggested methods to decrease the levels of EKE in numerical
470 simulations. Backeberg et al. [2009] improved the representation of the southern Agulhas
471 Current by applying a higher-order momentum advection scheme, resulting in a well-
472 defined meandering current rather than a continuous stream of eddies. Anderson et al.
473 [2011] found that the use of relative wind forcing significantly decreased eddy intensities
474 and a study by Renault et al. [2017] focused on the current stress feedback between the
475 ocean and atmosphere, demonstrated a reduction of mesoscale variability by coupling the
476 ocean model with an atmospheric model. Improving the mesoscale variability in HYCOM
477 could therefore yield better results for the transport proxy, specifically for the offshore
478 regression models, in the future. In order to effectively mirror the performance of the *in*
479 *situ* transport proxy [Beal and Elipot, 2016], a numerical model that accurately simulates
480 Agulhas meanders and the vertical variability, including an accurate representation of the
481 Agulhas Undercurrent is required and this has not yet been achieved in existing regional
482 configurations.

483 The development of the ACT transport proxy was initially tested using a regional NEMO
484 configuration in order to evaluate the potential of the altimeter proxy to monitor the
485 multi-decadal transport of the Agulhas Current [van Sebille et al., 2010]. Using the
486 numerical model, it was concluded that the correlation between the Agulhas Current
487 transport and gradient in sea surface height was greater than $r=0.78$ for any three-year
488 measuring period, and is therefore an adequate timescale to build an accurate transport
489 proxy [van Sebille et al., 2010].

490 The HYCOM output in this study was used to test the sensitivity of the relationship
491 between transport and SSH slope over a range of time periods. It was hypothesised that

492 building the linear relationship over longer time periods, >3 years, would increase the skill
493 of the transport proxy, since the linear relationship would include more current variability
494 over longer periods of time. The results showed that calculating the transport proxy over
495 longer or shorter time periods did not necessarily improve the performance of the proxy,
496 thereby suggesting that the current dynamics for any 3-year period in the model could be
497 very similar, in agreement with the results obtained in van Sebille et al. [2010], suggesting
498 that the results were consistent despite the model biases. This suggests that 3-years is
499 an appropriate time-period to develop the transport proxy of the Agulhas Current in
500 HYCOM.

501 Lastly, the study showed that the transport proxy is sensitive to subsurface variability in
502 the model, hence caution should be taken regarding the implicit assumption of a fixed
503 vertical current structure. The accuracy of the transport proxy remains sensitive to model
504 bias. Hence the sensitivity of the proxy should be tested in other model simulations.
505 Sensitivity studies of this kind, using numerical ocean models, provide useful information
506 advancing our understanding of the sensitivities and limitations of transport proxies,
507 contributing to the improvement of long-term ocean monitoring approaches and assisting
508 in the development and planning of future measurement programmes.

509 **Authors contributions*

510 E.V. conducted the data analyses and wrote up the final paper. B.B provided the HYCOM
511 model data, supervised the project and provided financial support. J.H. supervised the
512 project and provided financial support and S.E. assisted with the methodology of the
513 transport proxy. All authors helped to conceptualize ideas and contributed to writing the
514 paper.

515 We have no conflicts of interest to disclose.

516 **Acknowledgements*

517 This work has been funded by the National Research Foundation of South Africa and
518 by the bilateral South Africa-Norway SANCOOP SCAMPI project. We would like to
519 thank the Nansen-Tutu Centre in South Africa and SAEON for providing opportunities
520 to present the project locally and internationally. We thank the Nansen Environmental
521 Remote Sensing Centre (NERSC) in Bergen, Norway, for hosting us for a duration of
522 the project and wish to thank Dr. Knut-Arild Lisæter for his guidance while working at
523 NERSC. We gratefully acknowledge Professor Lisa Beal, Dr. Shane Elipot and the rest of
524 the ASCA team from the Rosenstiel School of Marine and Atmospheric Science (RSMAS),
525 University of Miami, for granting us permission to replicate the Agulhas transport proxy
526 methods. Shane Elipot was supported by the U.S. National Science Foundation through
527 the ASCA project, Award OCE-1459543.

528 **References**

- 529 Anderson, L. A., McGillicuddy, D. J., Maltrud, M. E., Lima, I. D., and Doney, S. C.: Im-
530 pact of eddy-wind interaction on eddy demographics and phytoplankton community
531 structure in a model of the North Atlantic Ocean, *Dynamics of Atmospheres and*
532 *Oceans*, 52, 80–94, <https://doi.org/10.1016/j.dynatmoce.2011.01.003>, 2011.
- 533 Andres, M., Park, J.-H., Wimbush, M., X-H, Z., Chang, K., and Ichikawa, H.: Study
534 of the Kuroshio / Ryukyu Current System Based on Satellite-Altimeter and in situ
535 Measurements, *Journal of Oceanography*, 64, 937–950, 2008.
- 536 Backeberg, B. C., Johannessen, J. A., Bertino, L., and Reason, C. J.: The greater Agulhas
537 Current system: An integrated study of its mesoscale variability, *Journal of Physical*
538 *Oceanography*, 1, 29–44, 2008.
- 539 Backeberg, B. C., Bertino, L., and Johannessen, J. A.: Evaluating two numerical advec-
540 tion schemes in HYCOM for eddy-resolving modelling of the Agulhas Current, *Ocean*
541 *Science*, pp. 173–190, 2009.
- 542 Backeberg, B. C., Penven, P., and Rouault, M.: Impact of intensified Indian Ocean winds
543 on mesoscale variability in the Agulhas system, *Nature Climate Change*, 2, 608–612,
544 <https://doi.org/10.1038/nclimate1587>, 2012.
- 545 Backeberg, B. C., Counillon, F., Johannessen, J. a., and Pujol, M. I.: Assimilating along-
546 track SLA data using the EnOI in an eddy resolving model of the Agulhas system,
547 *Ocean Dynamics*, pp. 1121–1136, <https://doi.org/10.1007/s10236-014-0717-6>, 2014.
- 548 Beal, L. M. and Elipot, S.: Broadening not strengthening of the Agulhas Current since
549 the early 1990s, *Nature Publishing Group*, 540, 570–573, [https://doi.org/10.1038/](https://doi.org/10.1038/nature19853)
550 [nature19853](https://doi.org/10.1038/nature19853), 2016.
- 551 Beal, L. M., De Ruijter, W. P. M., Biastoch, A., and Zahn, R.: On the role of the
552 Agulhas system in ocean circulation and climate., *Nature*, 472, 429–36, [https://doi.org/](https://doi.org/10.1038/nature09983)
553 [10.1038/nature09983](https://doi.org/10.1038/nature09983), 2011.
- 554 Beal, L. M., Elipot, S., Houk, A., and Leber, G. M.: Capturing the Transport Variability
555 of a Western Boundary Jet: Results from the Agulhas Current Time-Series Experiment

556 (ACT)*, *Journal of Physical Oceanography*, 45, 1302–1324, <https://doi.org/10.1175/>
557 JPO-D-14-0119.1, 2015.

558 Biastoch, A. and Krauss, W.: The Role of Mesoscale Eddies in the Source Regions of the
559 Agulhas Current, *Journal of Physical Oceanography*, 29, 2303–2317, 1999.

560 Birol, F., Fuller, N., Lyard, F., Cancet, M., Nino, F., Delebecque, C., Fleury, S., Toubanc,
561 F., Melet, A., Saraceno, M., et al.: Coastal applications from nadir altimetry: Example
562 of the X-TRACK regional products, *Advances in Space Research*, 59, 936–953, 2017.

563 Bleck, R.: An oceanic general circulation model framed in hybrid isopycnic-Cartesian
564 coordinates, 37, 55–88, 2002.

565 Braby, L., Backeberg, B. C., Ansorge, I., Roberts, M. J., Krug, M., and Reason, C. J. C.:
566 Observed eddy dissipation in the Agulhas Current, *Geophysical Research Letters*, 43,
567 8143–8150, <https://doi.org/10.1002/2016GL069480>, 2016.

568 Cai, W.: Antarctic ozone depletion causes an intensification of the Southern Ocean
569 super-gyre circulation, *Geophysical Research Letters*, 33, 1–4, <https://doi.org/10.1029/>
570 2005GL024911, 2006.

571 Chassignet, E. P., Hurlburt, H. E., Martin, O., Halliwell, G. R., Hogan, P. J., Wallcraft,
572 A. J., Baraille, R., and Bleck, R.: The HYCOM (HYbrid Coordinate Ocean Model) data
573 assimilative system, 65, 60–83, <https://doi.org/10.1016/j.jmarsys.2005.09.016>, 2007.

574 Chelton, D. B., DeSzoeke, R. A., Schlax, M. G., El Naggar, K., and Siwertz, N.: Geograph-
575 ical Variability of the First Baroclinic Rossby Radius of Deformation, *Journal of Phys-*
576 *ical Oceanography*, 28, 433–460, [https://doi.org/10.1175/1520-0485\(1998\)028<0433:](https://doi.org/10.1175/1520-0485(1998)028<0433:)
577 [GVOTFB>2.0.CO;2](https://doi.org/10.1175/1520-0485(1998)028<0433:GVOTFB>2.0.CO;2), 1998.

578 de Ruijter, W. P. M., van Leeuwen, P. J., and Lutjeharms, J. R. E.: Generation and
579 Evolution of Natal Pulses: Solitary Meanders in the Agulhas Current, *Journal of Phys-*
580 *ical Oceanography*, 29, 3043–3055, [https://doi.org/10.1175/1520-0485\(1999\)029<3043:](https://doi.org/10.1175/1520-0485(1999)029<3043:)
581 [GAEONP>2.0.CO;2](https://doi.org/10.1175/1520-0485(1999)029<3043:GAEONP>2.0.CO;2), 1999.

582 Dee, D. P., Uppala, S. M., Simmons, A. J., Berrisford, P., Poli, P., Kobayashi, S., Andrae,
583 U., Balmaseda, M. A., Balsamo, G., Bauer, P., Bechtold, P., Beljaars, A. C. M., Berg,

584 L. V. D., Bidlot, J., Bormann, N., Delsol, C., Dragani, R., Fuentes, M., Geer, A. J.,
585 and Dee, D. P.: The ERA-Interim reanalysis : configuration and performance of the
586 data assimilation system, pp. 553–597, <https://doi.org/10.1002/qj.828>, 2011.

587 Dijkstra and de Ruijter, W.: On the Physics of the Agulhas Current : Steady Retroflection
588 Regimes, *Journal of Physical Oceanography*, 31, 2971–2985, 2001.

589 Durgadoo, J., Loveday, B., Reason, C., Penven, P., and Biastoch, A.: Agulhas Leakage
590 Predominantly Responds to the Southern Hemisphere Westerlies, *Journal of Physical*
591 *Oceanography*, 43, 2113–2131, <https://doi.org/10.1175/JPO-D-13-047.1>, 2013.

592 Elipot, S. and Beal, L.: Characteristics , Energetics , and Origins of Agulhas Current
593 Meanders and their Limited Influence on Ring Shedding, *Journal of Physical Oceano-*
594 *graphy*, 45, 2294—2314, 2015.

595 Fu, L.-L., Chelton, D., Le Traon, P.-Y., and Morrow, R.: Eddy Dynamics From Satellite
596 Altimetry, *Oceanography*, 23, 14–25, <https://doi.org/10.5670/oceanog.2010.02>, 2010.

597 George, M. S., Bertino, L., O.M, J., and A, S.: Validation of a hybrid coordinate
598 ocean model for the Indian Ocean, *Journal of Operational Oceanography*, 3, 25–38,
599 <https://doi.org/10.1080/1755876X.2010.11020115>, 2010.

600 Gordon, A. L.: Oceanography: The brawniest retroflection, *Nature*, 421, 904–905,
601 <https://doi.org/10.1038/421904a>, 2003.

602 Gordon, A. L., Lutjeharms, J. R., and Gründlingh, M. L.: Stratification and circulation at
603 the Agulhas Retroflection, *Deep Sea Research Part A. Oceanographic Research Papers*,
604 34, 565–599, [https://doi.org/10.1016/0198-0149\(87\)90006-9](https://doi.org/10.1016/0198-0149(87)90006-9), 1987.

605 Hermes, J. C., Reason, C., and Lutjeharms, J.: Modeling the Variability of the Greater
606 Agulhas Current System, *Journal of climate*, 20, 3131–3146, <https://doi.org/10.1175/JCLI4154.1>, 2007.

608 Holton, L., Deshayes, J., Backeberg, B., Loveday, B., Hermes, J., and Reason, C.: Spatio-
609 temporal characteristics of Agulhas leakage: a model inter-comparison study, *Climate*
610 *dynamics*, 48, 2107–2121, 2017.

611 Imawaki, S., Uchida, H., Ichikawa, H., and Fukasawa, M.: Satellite altimeter monitoring
612 the Kuroshio transport south of Japan, *Geophysical Research Letters*, 28, 17–20, 2001.

613 Loveday, B. R., Durgadoo, J. V., Reason, C. J., Biastoch, A., and Penven, P.: Decoupling
614 of the Agulhas leakage from the Agulhas Current, *Journal of Physical Oceanography*,
615 44, 1776–1797, <https://doi.org/10.1175/JPO-D-13-093.1>, 2014.

616 Lutjeharms, J. R. E.: *The Agulhas Current*, 2006.

617 Maul, G. A., Mayer, D. A., and Bushnell, M.: Statistical relationships between local sea
618 level and weather with Florida-Bahamas cable and Pegasus measurements of Florida
619 Current volume transport, *Journal of Geophysical Research*, 95, 3287–3296, 1990.

620 Penven, P., Herbette, S., and Rouault, M.: Ocean Modelling in the Agulhas Current
621 System, in: *Nansen-Tutu Conference Proceedings*, pp. 17–21, [https://doi.org/10.1017/](https://doi.org/10.1017/CBO9781107415324.004)
622 [CBO9781107415324.004](https://doi.org/10.1017/CBO9781107415324.004), 2011.

623 Reason, C. J. C.: Subtropical Indian Ocean SST dipole events and southern African
624 rainfall, *Geophysical Research Letters*, 28, 2225–2227, 2001.

625 Renault, L., McWilliams, J. C., Penven, P., Renault, L., McWilliams, J. C., and Pen-
626 ven, P.: Modulation of the Agulhas Current Retroflexion and Leakage by Oceanic
627 Current Interaction with the Atmosphere in Coupled Simulations, *Journal of Physical*
628 *Oceanography*, 47, 2077–2100, <https://doi.org/10.1175/JPO-D-16-0168.1>, 2017.

629 Rouault, M. and Lutjeharms, J.: Estimation of sea-surface temperature around southern
630 Africa from satellite-derived microwave observations., *South African journal of science*,
631 99, 489–493, 2003.

632 Rouault, M., White, S. A., Reason, C. J. C., Lutjeharms, J. R. E., and Jobard, I.:
633 Ocean Atmospheric Interaction in the Agulhas Current Region and a South African
634 Extreme Weather Event, *Weather and Forecasting*, 17, 655–669, [https://doi.org/10.](https://doi.org/10.1175/1520-0434(2002)017<0655:OAIITA>2.0.CO;2)
635 [1175/1520-0434\(2002\)017<0655:OAIITA>2.0.CO;2](https://doi.org/10.1175/1520-0434(2002)017<0655:OAIITA>2.0.CO;2), 2002.

636 Rouault, M. J. and Penven, P.: New perspectives on Natal Pulses from satellite ob-
637 servations, *Journal of Geophysical Research: Oceans*, 116, 1–14, [https://doi.org/](https://doi.org/10.1029/2010JC006866)
638 [10.1029/2010JC006866](https://doi.org/10.1029/2010JC006866), 2011.

639 Rouault, M. J., Mouche, A., Collard, F., Johannessen, J. A., and Chapron, B.: Mapping
640 the Agulhas Current from space : An assessment of ASAR surface current velocities,
641 Journal of Geophysical Research, 115, 1–14, <https://doi.org/10.1029/2009JC006050>,
642 2010.

643 Smith, L., , Boudra, D., and R, B.: A Wind-Driven Isopycnic Coordinate Model of the
644 North and Equatorial Atlantic Ocean 2 . The Atlantic Basin Experiments, Journal of
645 Geophysical Research, 95, 105–128, 1990.

646 Sprintall, J. and Revelard, A.: The Indonesian Throughflow response to Indo-Pacific
647 climate varaibility, Journal of Geophysical Research: Oceans, 119, 1161–1175,
648 <https://doi.org/10.1002/2013JC009533>.Received, 2014.

649 Tsugawa, M. and Hasumi, H.: Generation and Growth Mechanism of the Natal
650 Pulse, Journal of Physical Oceanography, 40, 1597–1612, [https://doi.org/10.1175/
651 2010JPO4347.1](https://doi.org/10.1175/2010JPO4347.1), 2010.

652 Uppala, S. M., Kallberg, P. W., Simmons, A. J., Andrae, U., Bechtold, V. D. C., Fiorino,
653 M., Gibson, J. K., Haseler, J., Hernandez, A., Kelly, G. A., Li, X., Onogi, K., Saarinen,
654 S., Sokka, N., Allan, R. P., Andersson, E., Arpe, K., Balmaseda, M. A., Beljaars, A.
655 C. M., Berg, L. V. D., Bidlot, J., Bormann, N., Caires, S., Chevallier, F., Dethof,
656 A., Dragosavac, M., Fisher, M., Fuentes, M., Hagemann, S., Holm, E., Hoskins, B. J.,
657 Isaksen, L., Janssen, P. A. E. M., Jenne, R., Mcnally, A. P., Mahfouf, J., Morcrette,
658 J., Rayner, N. A., Saunders, R. W., Simon, P., Sterl, A., Trenberth, K. E., Untch, A.,
659 Vasiljevic, D., Viterbo, P., and Woollen, J.: The ERA-40 re-analysis, Quarterly Journal
660 of the Royal Meteorological Society, 131, 2961–3012, <https://doi.org/10.1256/qj.04.176>,
661 2005.

662 van Sebille, E., Beal, L. M., and Biastoch, A.: Sea surface slope as a proxy for
663 Agulhas Current strength, Geophysical Research Letters, 37, 2–5, [https://doi.org/
664 10.1029/2010GL042847](https://doi.org/10.1029/2010GL042847), 2010.

665 Yan, X. M. and Sun, C.: An altimetric transport index for Kuroshio inflow northeast
666 of Taiwan Island, Science China Earth Sciences, 58, 697–706, [https://doi.org/10.1007/
667 s11430-014-5024-z](https://doi.org/10.1007/s11430-014-5024-z), 2015.

- 668 Yang, H., Lohmann, G., Wei, W., Dima, M., Ionita, M., and Liu, J.: Intensification
669 and poleward shift of subtropical western boundary currents in a warming climate,
670 Journal of Geophysical Research: Oceans, 121, 4928–4945, [https://doi.org/10.1002/](https://doi.org/10.1002/2015JC010796)
671 2015JC010796, 2016.
- 672 Zhu, X. H., Ichikawa, H., Ichikawa, K., and Takeuchi, K.: Volume transport variability
673 southeast of Okinawa Island estimated from satellite altimeter data, Journal of Ocean-
674 ography, 60, 953–962, <https://doi.org/10.1007/s10872-005-0004-8>, 2004.